Geophysical Journal International

Geophys. J. Int. (2013) doi: 10.1093/gji/ggt265

Geophysical Journal International Advance Access published July 30, 2013

Decarbonation and thermal microcracking under magmatic *P-T-f*CO_2 conditions: the role of skarn substrata in promoting volcanic instability

S. Mollo,[1] M. J. Heap,[2] D. B. Dingwell,[3] K.-U. Hess,[3] G. Iezzi,[4] M. Masotta,[5] P. Scarlato[1] and S. Vinciguerra[6,7]

[1]*Istituto Nazionale di Geofisica e Vulcanologia (INGV), Via di Vigna Murata,* 605, 00143 *Rome, Italy. E-mail: mollo@ingv.it*
[2]*Laboratoire de Déformation des Roches, Équipe de Géophysique Expérimentale, Institut de Physique de Globe de Strasbourg, UMR* 7516 *CNRS, EOST, Université de Strasbourg, Strasbourg, France*
[3]*Earth and Environment, LMU – University of Munich, Theresienstr.* 41*/III,* 80333 *Munich, Germany*
[4]*Dipartimento INGEO, Università G. d'Annunzio, Chieti, Italy*
[5]*Bayerisches Geoinstitut, Universität Bayreuth, Bayreuth, Germany*
[6]*Department of Geology, University of Leicester, University Road, Leicester,* LE1 7RH*, UK*
[7]*British Geological Survey, Environmental Science Centre, Keyworth, Nottingham,* NG12 5GG*, UK*

Accepted 2013 July 4. Received 2013 June 30; in original form 2013 March 25

SUMMARY

We present a systematic study on the influence of pressure (0.1–600 MPa), temperature (750–1200 °C), carbon dioxide fugacity (logfCO_2 = −4.41 to 3.60) and time (2–12 hr) on the chemical and physical properties of carbonate rock. Our experiments aim to reproduce the conditions at the periphery of magma chamber where carbonate host rock is influenced by, but not readily assimilated by, magma. This permits the investigation of the natural conditions at which circulating fluids/gases promote infiltration reactions typical of metasomatic skarns that can involve large volumes of subvolcanic carbonate basements. Results show that, providing that carbon dioxide is retained in the pore space, decarbonation does not proceed at any magmatic pressure and temperature. However, when the carbon dioxide is free to escape, decarbonation can occur rapidly and is not hindered by a low initial porosity or permeability. Together with carbon dioxide and lime, portlandite, a mineral commonly found in voluminous metasomatic skarns, readily forms during carbonate decomposition. Post-experimental analyses highlight that thermal microcracking, a result of the highly anisotropic thermal expansion of calcite, exerts a greater influence on rock physical properties (porosity, ultrasonic wave velocities and elastic moduli) than decarbonation. Our data suggest that this will be especially true at the margins of dykes or magma bodies, where temperatures can reach up to 1200 °C. However, rock compressive strength is significantly reduced by both thermal cracking and decarbonation, explained by the relative weakness of lime + portlandite compared to calcite, and an increase in grain size with increasing temperature. Metasomatic skarns, whose petrogenetic reactions may involve a few tens of cubic kilometres, could therefore represent an important source of volcanic instability.

Key words: Phase transitions; Effusive volcanism; Volcanic hazards and risks.

1 INTRODUCTION

The impact of heat, readily provided by magma (e.g. Wohletz *et al.* 1999; Civetta *et al.* 2004; Bonaccorso *et al.* 2010) and/or circulating hot fluids (e.g. Merle *et al.* 2010; Siniscalchi *et al.* 2010), on carbonate volcanic substrata has recently been highlighted as an important consideration in volcanic hazard assessment (Mollo *et al.* 2011, 2012; Heap *et al.* 2013a). The significant rock volumes (>1 km^3) at risk imply that the thermally activated weakening (a consequence of both chemical alteration and thermal cracking) of a carbonate volcanic substratum could play an important role in dictating large-scale volcano instability (Heap *et al.* 2013a; see also Van Wyk de Vries & Borgia 1996, 1997; Merle & Borgia 1996). The presence of large, subvolcanic carbonate sedimentary successions within volcanic systems is common in active volcanoes worldwide, e.g. Mt Etna (Italy; Lentini 1982), Mt Vesuvius (Italy; Bruno *et al.* 1998), the Colli Albani volcanic district (Italy; Gaeta *et al.* 2006), the Campi Flegrei volcanic district (Italy; D'Antonio

2011), Popocatépetl volcano (Mexico; Goff *et al.* 2001), the Colima volcanic complex (Mexico; Norini *et al.* 2010) and Merapi (Indonesia; Troll *et al.* 2012). For example, the influence of high temperatures on the chemical, physical and mechanical properties of the carbonate subvolcanic basement at Mt Etna can support the interpretation of (1) the irregularly low seismic velocity zones present beneath the volcanic edifice, (2) the anomalously high CO_2 degassing observed, (3) the anomalously high V_p/V_s ratios and the rapid migration of fluids and (4) the increasing flank instability (Heap *et al.* 2013a). Decarbonation ($CaCO_3 \rightarrow CaO + CO_2$) and thermal microcracking are likely to be the primary weakening mechanisms (Mollo *et al.* 2012) although, in the presence of clays, dehydroxylation can also occur (Mollo *et al.* 2011). Thermal- and pressure-induced ductility that can occur at relatively moderate temperatures and pressures due to the low shear stress required to initiate mechanical twinning and dislocation slip in calcite may also be a key factor in explaining the large-scale deformation observed at Mt Etna volcano (Heap *et al.* 2013a).

To date, the experiments in the above-mentioned studies were all performed at ambient pressure and under a limited range of experimental temperatures (up to 800 °C). Further experiments, designed to investigate the role of carbon dioxide fugacity (fCO_2), a factor that can severely influence the progression of decarbonation (Mollo *et al.* 2012), were also performed at a temperature of 750 °C. There is a close relationship between the partial pressure of CO_2 and the temperature of carbonate decomposition and melting (Chase 1998): (i) the decomposition temperature increases significantly (from 600 to 1250 °C) with increasing partial pressure of CO_2 (Treiman & Essene 1983; Samtani *et al.* 2002; Mollo *et al.* 2012) and, (ii) in the system $CaO + CO_2 + H_2O$, the melting temperature of calcite increases from 650 to 1240 °C as the partial pressure of CO_2 is increased from 0 to 40 MPa (Wyllie & Tuttle 1960). Here we expand the range of experimental temperatures permitting us to systematically investigate the potentially complex interplay between decarbonation and thermal microcracking.

The influence of pressure, temperature and fCO_2 on the fraction of carbonate decomposed, and its resultant impact on rock physical properties, is still poorly understood. Here we report on a systematic study on the influence of temperature (750–1200 °C) on carbonate rock. Our experiments were conducted over a range of pressure (0.1–600 MPa) and fCO_2 ($\log fCO_2 = -4.41$ to 3.60) conditions, at two experimental durations (2 and 12 hr). Our experimental conditions were designed to greatly expand the conditions used by previous studies (Mollo *et al.* 2011, 2012; Heap *et al.* 2013a) and to cover the range of conditions that are commonly extant in active volcanic systems. Following experimentation, our run products were systematically characterized in terms of their chemical and physical properties. We use these data to discuss the role of high temperatures in the stability of volcanoes containing carbonate substrata. We note at the outset that although we are aware that the proximity of magma and carbonate can lead to carbonate ingestion or 'assimilation' (e.g. Wenzel *et al.* 2002; Barnes *et al.* 2005; Gaeta *et al.* 2006, 2009; Piochi *et al.* 2006; Chadwick *et al.* 2007; Iacono-Marziano *et al.* 2007; Freda *et al.* 2005, 2008; Deegan *et al.* 2010; Mollo *et al.* 2010; Di Rocco *et al.* 2012; Troll *et al.* 2012), in this study we only consider the impact of high temperatures (under various conditions) on carbonate host rock. This allows permits that investigation of the natural conditions at which circulating fluids/gases promote infiltration reactions typical of metasomatic skarns that involve large volumes (a few tens of cubic kilometres) of subvolcanic carbonate basements (e.g. Di Rocco *et al.* 2012).

2 MATERIALS AND METHODS

2.1 Experimental material

The rock used throughout this study is a micritic limestone from Solnhofen (Bavaria, Germany), hereafter referred to as SLN. Due to its fine grain size, homogeneity, experimental reproducibility and chemical purity (99.9 wt. per cent calcite) SLN has been extensively used in rock deformation studies (e.g. Rutter 1974; Schubnel *et al.* 2005). Moreover, SLN chemical composition closely matches to that of limestones from sedimentary substrata under active volcanoes (e.g. Heap *et al.* 2013a). For the same reasons, and due to the volume of pre-existing data, SLN represents an ideal rock type for our study. The SLN used in this study has an initial porosity (Φ) of 4.55 per cent (±0.1 per cent), a mean grain size of 5 μm and *P*- (V_p) and *S*-wave (V_s) velocities of 5.64 and 3.05 km s^{-1}, respectively. Chemical analyses indicated that the content of calcite and CaO in our SLN is ∼99.9 and ∼55 wt. per cent, respectively.

2.2 Experimental conditions

As noted, our experimental conditions were designed to greatly expand the conditions used by previous studies (Mollo *et al.* 2011, 2012; Heap *et al.* 2013a) and to cover the range of conditions that are commonly extant in active volcanic systems. The rationale behind our experimental conditions is presented below, and a complete experimental condition summary is available in Table S1.

Our experiments were conducted at confining pressures (P_c) of 0.1, 150 or 600 MPa. These pressures were chosen to investigate the thermal decomposition of carbonate rocks at or near shallow (<1 km) and deep (∼18 km) magma chambers. The experimental temperatures were determined on the basis of preliminary thermogravimetric (TG) analyses conducted in a pure air atmosphere. Our data show that, SLN decomposes from 717 to 862 °C at 0.1 MPa (atmospheric pressure), and that the onset temperature (T_{onset}) of the decarbonation reaction is about 780 °C (Fig. 1). On this basis, we have chosen experimental temperatures of 750 and 810 °C

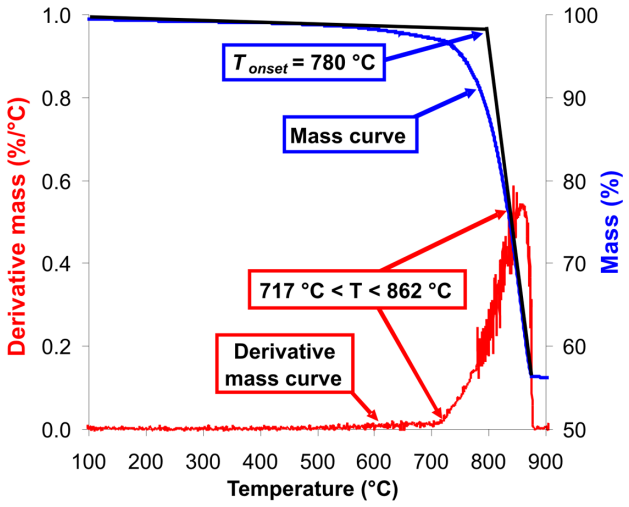

Figure 1. Thermogravimetric (TG, the blue curve) and differential thermogravimetric (DTG, the red curve) curves for an 'as-collected' powdered sample of Solnhofen limestone. The 'onset temperature' (T_{onset}), a characteristic value related to the thermal decomposition of the material under the imposed conditions, is defined by the intersection of the two experimental data tangents (black lines).

(i.e. 30 °C below and above the T_{onset} of the decarbonation reaction, respectively). These temperatures are also relevant to those found within carbonate volcanic substrata close to magma bodies (e.g. Wohletz *et al.* 1999; Bonaccorso *et al.* 2010). An additional experimental temperature of 1200 °C was used to represent the direct contact temperature between magma and carbonate rock (e.g. a carbonate magma chamber sidewall, or the carbonate host rock in direct contact with a magmatic intrusion). It is worth stressing that, our experimental temperature of 1200 °C is 40 °C below the melting temperature of calcite, that is, 1240 °C (Irving & Wyllie 1973). In a 'closed' system, the melting of calcite is invariably congruent (producing a liquid with the same composition as the solid; Gillet *et al.* 1996; Ivanov & Deutsch 2002). However, in an 'open' system CO_2 is rapidly removed and CaO precipitates as primary phase due to its very high melting temperature of 2617 °C (Weast 1985; Lide *et al.* 1994).

The progression of carbonate decomposition in SLN samples is described by the decomposed fraction η_{dec} ranging from 0 to 1, that is, $\eta_{dec} = 1$ for a sample fully decomposed (see the Appendix for a more detailed discussion). Guided by our calcination analyses, we selected two experimental durations relevant for decarbonation: (i) 2 hr where η_{dec} reaches 0.21, 0.57 and 1.00 at 750, 810 and 1200 °C, respectively and (ii) 12 hr where η_{dec} is equal to 1.00 at any $T \geq 750$ °C. The experiments of this study were performed under controlled fCO_2 conditions ranging from $\log fCO_2 = -4.41$ to 3.6. This range reproduces the fCO_2 expected in: (i) an 'open' system where CO_2 is rapidly and efficiently removed ($\log fCO_2 = -4.41$) and (ii) a 'closed' system in which CO_2 is trapped under high-pressure conditions ($\log fCO_2 = -3.00$ to 3.6). Our fCO_2 interval also corresponds to the oxygen fugacities (i.e. $-\log fO_2 = 0.68$–15.60) commonly measured in volcanic systems characterized by intense CO_2 emissions (Gaeta *et al.* 2009; Mollo *et al.* 2012 and references therein). Notably, the fO_2 of a subvolcanic system strictly depends on the amount of CO_2, which can significantly change the fO_2 by several orders of magnitude (Wenzel *et al.* 2002; Gaeta *et al.* 2009; Di Rocco *et al.* 2012).

2.3 Decarbonation experiments

Both atmospheric ($P_c = 0.1$ MPa) and high-pressure decarbonation experiments ($P_c = 150$ and 600 MPa) were performed at the HP-HT Laboratory of experimental Volcanology and Geophysics of Istituto Nazionale di Geofisica e Vulcanologia (INGV, Rome, Italy).

Our experiments at 0.1 MPa (Experimental Set 1) were conducted in a Nabertherm RHTV vertical tube gas-mixing furnace. The fCO_2 (between $fCO_2 = -4.41$ and -1.01) was imposed using gas mixtures of pure CO + CO_2 + air that produced a variable $P^{ext}_{CO_2}$ with respect to the P_c of 0.1 MPa.

The fCO_2 was computed using the Peng–Robinson equation of state (Peng & Robinson 1976; Elliott & Lira 1999). It is worth noting that the behaviour of CO_2 at 0.1 MPa closely approximates that of an ideal gas, that is, $fCO_2 \cong P^{ext}_{CO_2}$. The fO_2 was monitored and maintained constant by means of an yttria-doped-zirconia solid electrolyte oxygen sensor and two digital thermal mass flow meters controlled via software. Each experiment was performed using two cylindrical samples of SLN (20 mm in diameter and 60 mm in length) inserted into a Pt-coil and suspended within the furnace. The target temperature (750, 810 or 1200 °C) was achieved using a constant heating rate of 10 °C min^{-1}; after the experiment (i.e. after 2 or 12 hr at the dwell temperature) the samples were cooled at the same rate. A Pt-crucible was also suspended within the furnace and loaded with 10 g of SLN (reduced to a powder and passed through a #200 mesh sieve). At the end of each experiment, one of the two cylindrical cores was then reduced to a powder with a grain size identical to that of the suspended powder. Subsequent chemical analysis of the two powders would yield valuable information on the influence of rock properties (e.g. porosity, grain size and permeability) on the decarbonation process (Yavuz et al. 2010). The remaining cylindrical core sample was used for systematic physical property characterization (see Section 3.2.4).

Our high-pressure experiments (Experimental Set 2) were performed at either 150 or 600 MPa in a piston cylinder apparatus equipped with an MgO-borosilicateglass-NaCl assembly (see Masotta *et al.* 2012 for further details). For each experiment, a Pt-capsule (5 mm in diameter and 10 mm in length) was loaded with 0.20 g of SLN powder and then sealed. Our high-pressure experiments were performed at temperatures of 750, 810 and 1200 °C, at durations of 2 as well as 12 hr, and at fCO_2 between 2.35 and 3.60. For our experiments at $P_c = 150$ and 600 MPa, the fCO_2 was calculated using a modified Redlich–Kwong equation of state (Holloway 1977; Flowers 1979). After each experiment, the retrieved Pt-capsule was frozen in liquid nitrogen and punctured with a needle while frozen. An immediate weight loss occurred on warming, indicative of CO_2 vaporization. Drying the capsule at 320 °C for at least 10 min resulted in a negligible weight loss of about 0.7 per cent, due to the loss of H_2O from the capsule.

2.4 Analytical techniques

The mass-loss-on-calcination analyses were performed in a Nabertherm LHT chamber furnace at the HP-HT Laboratory (INGV). For each experiment, 5 g of powdered SLN was loaded in a Pt-crucible and then heated at a rate of 10 °C min^{-1} to a target temperature of 1200 °C. The samples were then held at that temperature for 12 hr to ensure complete decarbonation, and the loss of mass was measured.

Calcimetry analyses were performed using a Dietrich–Frühling calcimeter at the Dipartimento di Scienze Geologiche of the University 'Roma Tre' in Rome. For each sample, 1 g of powdered SLN was dissolved in 15 ml of 6 N hydrochloric acid (density = 1.12 g cm^{-3}) and the amount of CO_2 released was measured using a volumetric method.

TG and differential thermogravimetric (DTG) analyses were carried out at the Department für Geo- und Umweltwissenschaften, Sektion Mineralogie, Petrologie and Geochemie of Ludwig Maximilians Universität in Munich (Germany) using a Netzsch STA 449 C thermobalance apparatus. Powdered SLN (approximately 40 mg) was heated in an air atmosphere using a Pt crucible (with lid) at a rate of 10 °C min^{-1} to a temperature of 100 °C. The samples were held at 100 °C for 60 min, to ensure complete dryness. Samples were then heated to a final target temperature of 1000 °C, again at 10 °C min^{-1}. TG analysis permits us to accurately measure the mass loss of the sample during controlled heating; and DTG is simply the rate of the loss of mass. Since our samples were dry, any loss in mass is the direct result of mineralogical changes to the sample as a consequence of the increasing temperature. In the case of pure limestone, TG and DTG will track the progression of decarbonation.

X-ray powder diffraction (XRPD) analysis was performed using the Siemens D-5005 diffractometer at the DIGAT department, Università G. d'Annunzio of Chieti (Italy). It operates in the vertical θ–2θ Bragg–Brentano configuration and is equipped with a

Ni-filtered Cu$K\alpha$ radiation. All data were collected in the 2θ range of 3°–70°, with a step scan of 0.02° and a counting time of 8 s per step. For each analysis, 10 mg of powdered sample was mounted into the central hole of a nominally zero-background Si-sample holder (Li & Albe 1993). The identification of crystalline phases for each pattern was performed using crystal models reported in the commercial inorganic crystal structure database (ICSD) allowing a better fit to the observed Bragg reflection (2θ positions and relative intensities). For each crystalline compound identified, the lattice parameters, atomic positions and space groups were then used for the successive Le Bail and Rietveld refinements (Young 1993; Le Bail 2005; Percharsky & Zavaliji 2005), both implemented in the EXPGUI-GSAS software package (Larson & von Dreele 1997; Toby 2001). For the former refinement method, the background was initially constrained manually and subsequently modelled by a polynomial Chebyshev function using five to 10 coefficients. Then, cell parameters for each crystalline phase and a constrained sample displacement parameter were refined. Bragg peak profiles were modelled using the function refining both Lorentzian (Lx, Ly) and Gaussian (GW) contributions (Finger *et al.* 1994). Each Le Bail refinement was terminated when the observed XRPD spectra were adequately reproduced. All these parameters were then kept fixed and used in the following Rietveld refinement, where only the scale factor was refined to obtain a quantitative phase analysis (QPA).

2.5 Physical property analyses

To assess the impact of decarbonation on rock physical properties under a variety of different experimental conditions (temperature, duration and fCO_2), we performed a systematic rock physical property characterization on both 'as-collected' SLN cylindrical core samples (i.e. samples that have undergone no deformation or thermal-stressing, 20 mm in diameter and about 60 mm in length) and the SLN cylindrical core samples (i.e. the samples that were not powdered, also 20 mm in diameter and about 60 mm in length, see above) from Experimental Set 1. Unfortunately, rock physical property analysis was not possible on the powdered samples of Experimental Set 2 (physical property measurements require an unpowdered cylindrical core sample).

Ultrasonic wave velocity measurements were conducted at the Laboratoire de Déformation des Roches (LDR, Université de Strasbourg) using an Agilent Technologies DSO5012A digital storage oscilloscope, an Agilent Technologies 33210A, 10 MHz function/waveform generator and two broad-band PZT piezoelectric transducer crystals (100 kHz to 1 MHz frequency) located at the top and bottom of the sample. Measurements were performed at ambient pressure and temperature, and used a force of 600 N to ensure a good contact between the endcaps and the sample. Heap *et al.* (2013a) showed that ultrasonic wave velocities from thermally stressed limestone samples (i.e. heated, cooled and then measured) were similar to those conducted at *in situ* temperatures (i.e. heated, measured and then cooled). Such behaviour is consistent with the fact that the decarbonation reaction is frozen-in at $T < 600$ °C (Fig. 1). Although we note that a recent study (Heap *et al.* 2013b) has shown that thermal microcracking can be more prevalent during the cooling cycle of a thermal stressing experiment; it is convincible that in the case of Heap *et al.* (2013a), the impact of decarbonation masked any additional thermal microcracking during cooling. Ultrasonic velocities were subsequently used to calculate the dynamic Young's modulus (E_d) and the dynamic Poisson's ratio (ν_d) according to Guéguen & Palciauskas (1994).

The connected porosity (Φ) of each sample was measured using both the triple-weight water saturation method (Guéguen & Palciauskas 1994) at the Laboratoire de Déformation des Roches (Strasbourg) and by an AccuPyc II 1340 helium pycnometer with an analytical accuracy of ±0.001 per cent at the HP-HT Laboratory of the INGV.

Uniaxial compressive strength (UCS) experiments were performed using the uniaxial press at the HP-HT Laboratory of the INGV. Samples were loaded at a constant strain rate of 5×10^{-5} s^{-1} until failure. Axial strain was continuously monitored during experimentation by means of an LVDT transducer, and axial stress by a load cell. UCS measurements were all performed at ambient temperature.

Microstructural observations were performed using the JEOL-JSM6500F Field Emission Gun — Scanning Electron Microscope (FE-SEM) located at the HP-HT Laboratory of the INGV.

3 RESULTS AND DISCUSSION

3.1 The path of the decarbonation reaction

The relationship between the fCO_2 and the fraction of carbonate decomposed (the η_{dec} value) is presented in Fig. 2. The data at $P_c = 0.1$ MPa and $fCO_2 = -4.41$ (i.e. under 'open' conditions), show the decarbonation reaction (A9) is dependent on both temperature and duration. While 12 hr is sufficient for complete decarbonation (i.e. $\eta_{dec} = 1$) at all experimental temperatures, a duration of 2 hr is only sufficient for a temperature of 1200 °C. The 2 hr experiments at 750 and 810 °C only reached η_{dec} values of 0.21 and 0.57, respectively (Fig. 2). These data indicate that, with respect to the timescale of magma–carbonate interaction processes (Freda *et al.* 2008), the kinetics of the decarbonation reaction is virtually instantaneous under

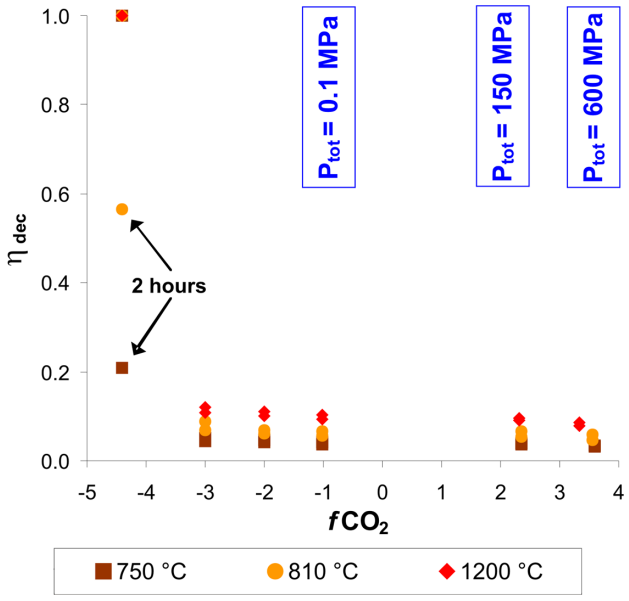

Figure 2. The progression of calcite decomposition as a function of carbon dioxide fugacity (fCO_2). The different symbols represent different experimental temperatures: brown squares, 750 °C; yellow circles, 810 °C; red diamonds, 1200 °C. The upper and lower symbols indicate the experimental duration of 12 and 2 hr, respectively.

'open' degassing conditions, even when the temperature (750 °C) is below the T_{onset} of carbonate decomposition (i.e. 780 °C, see Fig. 1).

However, the progression of decarbonation at $P_c = 0.1$ MPa is severely inhibited at higher values of fCO_2 (i.e. under 'closed' conditions; see also Mollo *et al.* 2012). For example, the η_{dec} value only reached 0.12 at 1200 °C after 12 hr (Fig. 2). A close inspection of the data reveals that η_{dec} values decrease as the fCO_2 is increased from −3.00 to −1.01. When P_c is increased to 150 and 600 MPa the fCO_2 of the system increases by many orders of magnitude and decarbonation is inhibited further (Fig. 2). Under 'closed' conditions, the interfaces between the calcite crystals and the external atmosphere quickly become saturated in CO_2 (i.e. $P^{eq}_{CO_2} = P^{ext}_{CO_2} = P_c$) and consequently the decarbonation reaction stalls at both high (1200 °C) and intermediate (750–810 °C) temperatures. Our data therefore demonstrate that, as long as CO_2 is retained in the pore space of carbonate rocks, the decarbonation reaction does not proceed at any pressure and temperature, implying that the results of Mollo *et al.* (2012) may be extended to a much wider range of conditions representative of magmatic systems.

Further, our data show that the progression of decarbonation is not significantly influenced by the initial rock properties. SLN has a much lower grain size, is much less permeable and has a much lower porosity than the limestones used in previous studies (Mollo *et al.* 2011, 2012; Heap *et al.* 2013a). As explained in the Methods section, we investigated the influence of initial rock properties on decarbonation by analysing the chemical composition of rock and powder decarbonated under the same conditions. Our chemical analyses showed that the amount of $CaCO_3$ decomposed in a cylindrical core were lower than that of the powdered sample, but only by ∼10 per cent. This means that, for the imposed experimental conditions, the microstructure (grain size, permeability and porosity) of SLN did not significantly limit the decarbonation reaction by retaining CO_2 liberated during $CaCO_3$ decomposition (Ninan *et al.* 1991; Samtani *et al.* 2002).

Fig. 3 shows how the chemical composition of SLN changes as the decarbonation reaction proceeds. According to reaction (A9), calcite decomposes to CO_2 and calcium oxide or 'lime' (CaO). We observe both of these reaction products in our experimental samples. First, we observe that the amount of CO_2 released during carbonate thermal decomposition increases as η_{dec} increases, reaching a maximum value of ∼43 wt. per cent when $\eta_{dec} = 1$. Secondly, our XRPD spectra show a diminishing peak for calcite (also seen in our DTG data) and the appearance of peaks for lime as η_{dec} increases (see insets in Fig. 3). However, we also observe another mineral phase in both our XRPD data and as an endothermic peak in our DTG data: portlandite ($Ca(OH)_2$). Portlandite is a hydrous hexagonal phase formed by the recombination of CaO with atmospheric water vapour (e.g. Mollo *et al.* 2011 and references therein). The appearance of portlandite in the system $Ca(OH)_2$-CaO-H_2O was determined to be at 810 °C by Wyllie & Tuttle (1960). This temperature was then revised to 780 °C (Wyllie & Raynor 1965). In a more recent study, Koster van Groos (1982) observed that portlandite is also a stable phase at about 630 °C. In presence of air, portlandite persists at 1047 °C due the extraordinary fast recombination reaction leading to the hydration of CaO (Dash *et al.* 2000). In contrast, under CO_2-saturated conditions, portlandite cannot form due to the high melting temperature of calcite (1240 °C) and in the absence of water vapour (Wyllie & Tuttle 1960). XRPD spectra show that portlandite coexists with lime from about $\eta_{dec} = 0.2$.

It is worth stressing that portlandite is a common mineral phase of skarn rocks formed during magma–carbonate interaction (Lentz 1999; Rosa & Martin 2010). Skarns are the result of magmatic,

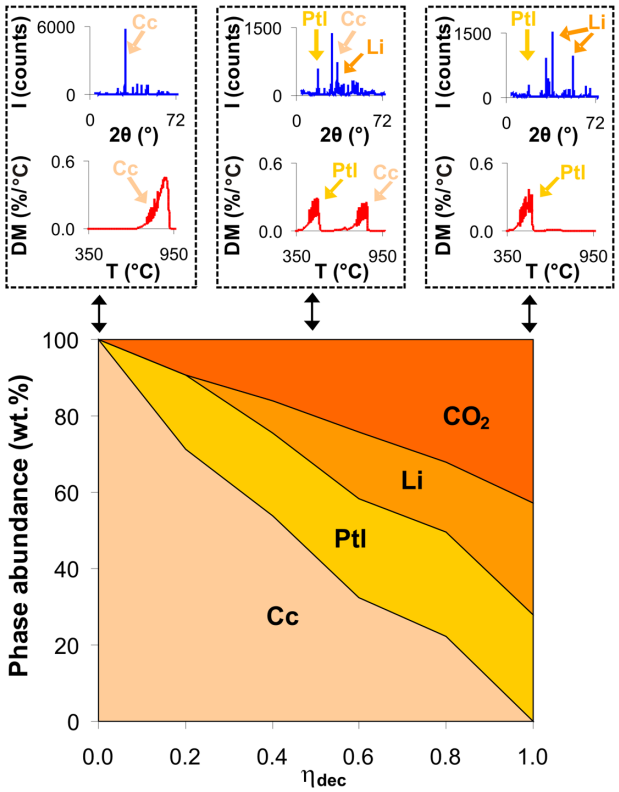

Figure 3. The evolution of Solnhofen limestone chemical composition as a function of decarbonation. Insets show both XRPD spectra and differential thermogravimetric (DTG) curves for selected stages of the process. Cc, calcite; Ptl, portlandite; Li, lime.

metasomatic and metamorphic reactions between magmas (or magmatic temperatures) and carbonate rocks. The periphery of magma chambers emplaced in carbonate materials are generally characterized by the presence of magmatic skarns that form between the magma and the carbonate wall-rocks (e.g. Di Rocco *et al.* 2012). Metasomatic skarns originate from fluid–rock interaction and, therefore, can involve large volumes of carbonate host rock because: (i) fluids/gases can easily infiltrate the fractured substrata and (ii) high temperatures can radiate up to several kilometres from the periphery of a magma chamber (e.g. Bonaccorso *et al.* 2010; Mollo *et al.* 2011). The presence of portlandite in our experimental run products is thus consistent with the idea that we have reproduced the natural conditions at which circulating fluids/gases promote infiltration reactions typical of skarn environments.

3.2 Changes in physical and mechanical properties

Standard rock characterization methods were employed as a tool to assess the impact of decarbonation under the various conditions implemented in this study. While the absolute values may not be representative of the *in situ* values (since our physical properties were measured under ambient pressures and temperatures, since they could not be measured during the decarbonation experiments), our data aim to show the trends and relationships between the physical properties and the progression of the decarbonation under the different conditions (temperature, duration and fCO_2).

Variations in physical and mechanical properties due to carbonate thermal decomposition have recently been reported in the literature

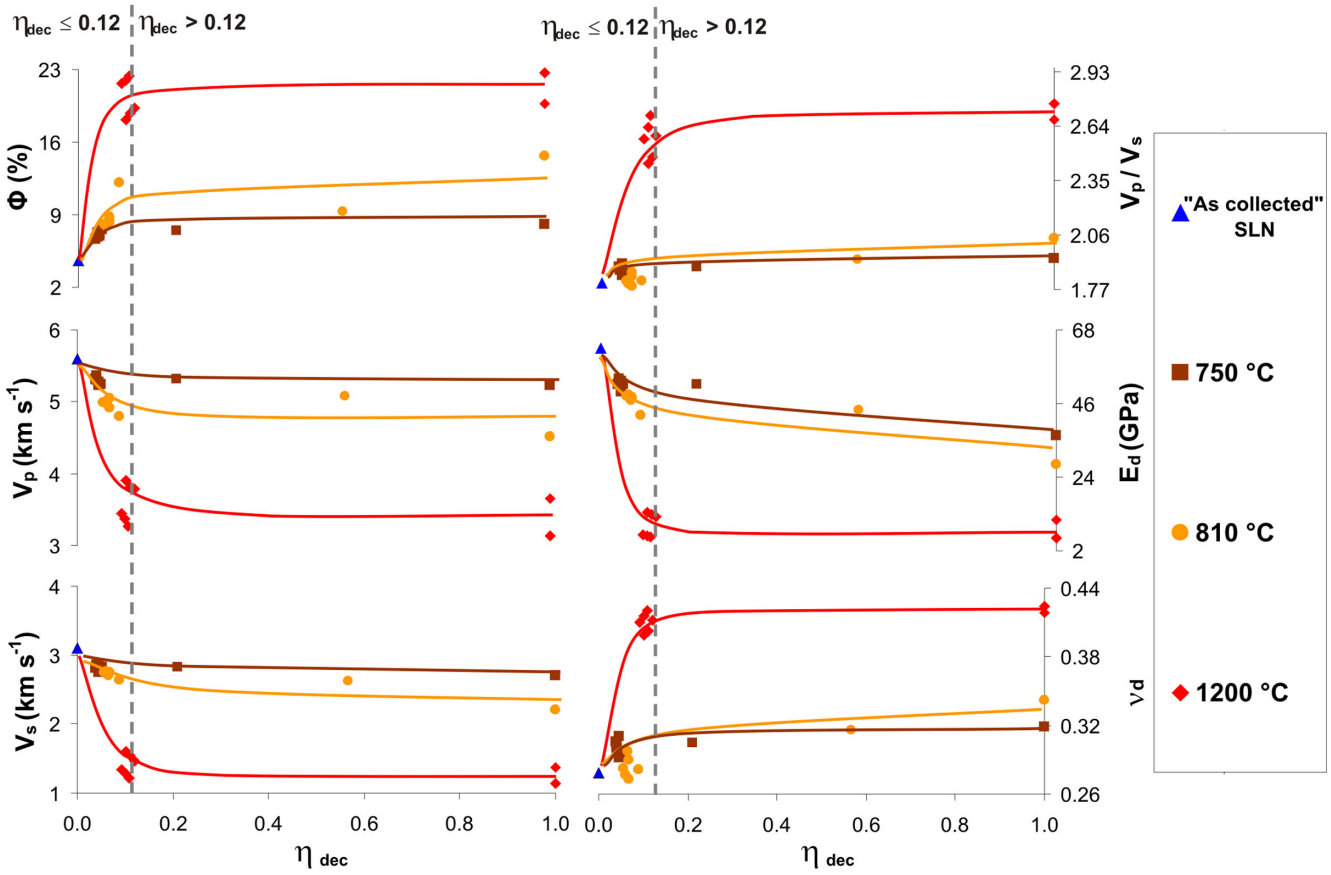

Figure 4. The evolution of rock physical properties (porosity, *P*-wave velocity, *S*-wave velocity, V_p/V_s ratio, dynamic Young's modulus and dynamic Poisson's ratio) as a function of decarbonation progression. The different symbols represent different experimental temperatures: blue triangles, 'as collected'; brown squares, 750 °C; yellow circles, 810 °C; red diamonds, 1200 °C.

(Mollo *et al.* 2011, 2012; Heap *et al.* 2013a) for some compositionally and texturally different carbonate-bearing rocks (a marly limestone, a pure limestone and a dolomite-bearing limestone). These studies highlighted that, as the decarbonation reaction progresses, the physical integrity of carbonate rocks is drastically compromised: porosity increases, while bulk density decreases, ultrasonic wave velocities, Young's modulus and strength all decrease too. Based on these data, these studies inferred that the decarbonation of a carbonate volcanic substratum could severely impact volcano stability. Further, it has been suggested that such changes in rock physical properties could help explain: (i) low seismic velocity zones present within carbonate substrata, (ii) anomalously high V_p/V_s ratios and the rapid migration of fluids, (iii) large-scale deformation of unstable flanks and (iv) the increasing instability of a volcanic edifice in the lifespan of a magmatic system (Heap *et al.* 2013a and references therein).

The evolution of rock physical properties with increasing η_{dec} are presented in Fig. 4 and parallel previous trends reported in previous studies dealing with carbonate thermal decomposition (Mollo *et al.* 2011, 2012; Heap *et al.* 2013a). This suggests that carbonate-bearing rocks of different initial chemical, textural and microstructural attributes are invariably weakened by decarbonation reactions. However, while the physical property data of Mollo *et al.* (2012) were measured for only one thermal-stressing temperature (750 °C), and therefore do not offer any information on their temperature dependence, in this study we show that the experimental temperature has a significant impact on rock physical properties, even at low values of η_{dec}. Fig. 4 shows that, at a constant level of decarbonation progression ($\eta_{dec} = 0.12$, that is, when the samples still contain 90 wt. per cent of calcite, see Fig. 3), an increase in temperature results in a dramatic increase in porosity, V_p/V_s ratio, and Poisson's ratio, and a dramatic decrease in ultrasonic wave velocities and Young's modulus. Notably, the increase of porosity from 4.55 to 22.69 per cent with increasing temperature (Fig. 4) is comparable to that observed during the petrogenetic evolution of skarns, that is, when the initial chemical and physical properties of carbonates are progressively altered by metasomatic reactions (Chobanu & Cook 2004). However, our experiments highlight that, at an early stage of the decarbonation reaction (i.e. $\eta_{dec} = 0.12$), the chemistry and mineralogy of the samples do not significantly change and only ~10 wt. per cent of calcite decomposes to CO_2 (Fig. 3). Therefore, we infer that the measured changes in rock physical properties (Fig. 4) are the result of pervasive thermal microcracking. Thermal microcracking is the consequence of the build-up of stress resulting from the anisotropic thermal expansion of calcite crystals. There have been many studies devoted to how the structure of calcite evolves with increasing temperature (e.g. Markgraf & Reeder 1985). The structure of calcite consists of alternating layers of calcium cations and CO_3 groups. Within any given layer each carbonate group has the same orientation, whereas within adjacent layers each carbonate group is rotated by 60°. An important structural aspect of calcite is that its thermal expansion is anisotropic, whereas most minerals

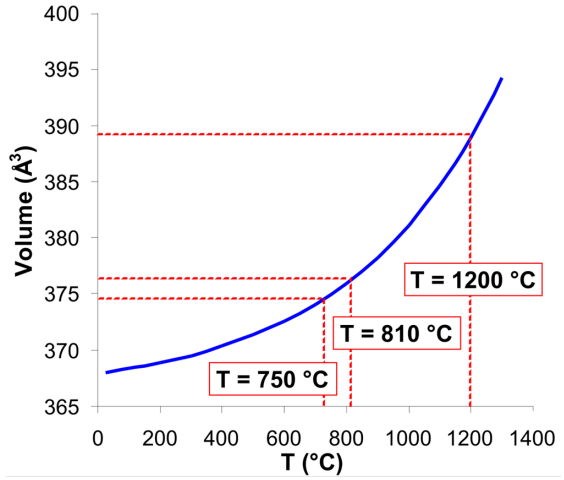

Figure 5. The thermal expansion of calcite as a function of temperature (using the data reported by Markgraf & Reeder 1985). The experimental temperatures (750, 810 and 1200 °C) have been indicated in the figure.

expand isotropically (Rao *et al.* 1968). In other rocks, it is usually the thermal expansion mismatch of the different mineral constituents that instigates thermal microcracking. Studies have shown that the *a*-axis of calcite contracts slightly as temperature increases, while the *c*-axis expands significantly (Rao *et al.* 1968; Markgraf & Reeder 1985; Dove & Powell 1989; Wu *et al.* 1995). Using the data reported by Markgraf & Reeder (1985), we have modelled the cell volume increase of calcite crystals as a function of temperature (Fig. 5). At the experimental temperatures of 750, 810 and 1200 °C the cell volume increases by 1.89, 2.15 and 5.68 per cent, respectively. The thermal expansion of calcite at the different experimental temperatures mirrors the evolution of physical properties with increasing temperature at $\eta_{dec} = 0.12$ (Fig. 4). It therefore seems likely that the increased thermal expansion results in a denser network of thermal microcracks, which then impact rock physical properties.

Our physical property changes at low values of η_{dec} are greater than those reported for a porous (32 per cent) bio-calcarenite (Mollo *et al.* 2012) at the same experimental temperature (750 °C). The microstructure of limestone has previously been identified as an important parameter for thermal microcracking (Homand-Etienne & Troalen 1984). Homand-Etienne & Troalen (1984) showed that a homogeneous, low-porosity carbonate rock (Carrara marble, 0 per cent porosity) was much more susceptible to thermal microcracking than a porous limestone (Crepey limestone, 10 per cent porosity) with a heterogeneous texture (ooliths, bioclasts and extraclasts). The microstructure of our experimental samples is similar to that of Carrara marble (although the grain size of Carrara marble is about 300 μm), and is therefore likely to be more susceptible to thermal microcracking (thermal microcracking initiated in Carrara marble at 200 °C). However, we note that thermal microcracking in Oakhall limestone (0.2 per cent porosity and a grain size of about 75 μm) initiated at temperatures above 500 °C (Fredrich & Wong 1986).

To qualify the hypothesis that thermal expansion of calcite and consequent microcracking are more prevalent at higher temperatures, we performed petrographic microscope observations and SEM microstructural analyses on an 'as-collected' SLN sample, as well as on samples taken to $\eta_{dec} \leq 0.12$ at temperatures of 750, 810 and 1200 °C (Fig. 6). As mentioned, we can rule out severe chemical changes as a result of decarbonation for samples at $\eta_{dec} \leq 0.12$ (Fig. 3). Examination using an optical microscope revealed that the grain size of SLN progressively increased as a function of temperature (Fig. 6). For example, at a temperature of 1200 °C the grain size was 8–10 μm (we recall that the 'as-collected' SLN has a mean grain size 5 μm). This observation is in agreement with the thermal expansion of calcite (Fig. 5). SEM analyses also indicate that 'as-collected' SLN is characterized by calcite crystals forming a dense mosaic. Small and sparse inter- and intracrystal cavities are also observed at the scale of the image (Fig. 6), accounting for the initial porosity of 4.55 per cent. However, we see an increasing number of thermal microcracks as the temperature is increased (Fig. 6), a result of the aforementioned thermal expansion of calcite (Fig. 5). At

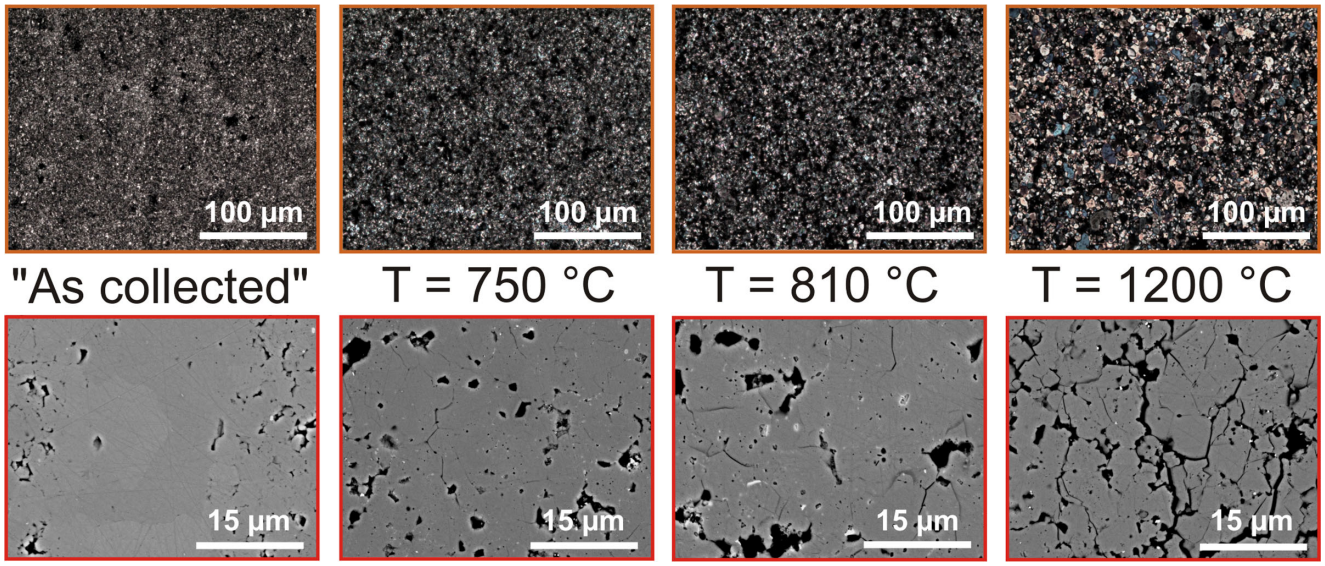

Figure 6. The impact of temperature on SLN microstructure (top pictures, optical photomicrographs; bottom pictures, SEM photomicrographs). All samples (with the exception of the 'as-collected' sample) were heated at the temperature indicated in the figure (750, 810 or 1200 °C) to a decarbonation progression of $\eta_{dec} = 0.12$. The optical photomicrographs were acquired under cross-polarized light, and the SEM photomicrographs in backscattered imaging mode.

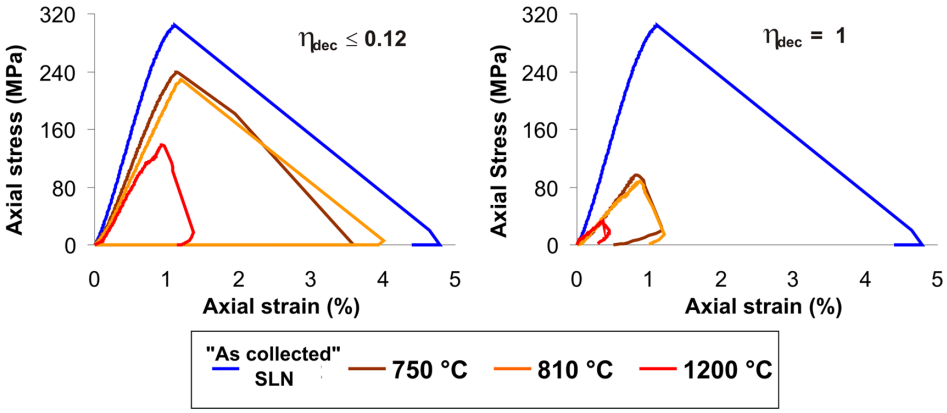

Figure 7. The influence of experimental temperature and decarbonation progression on the unconfined compressive strength (UCS) of Solnhofen limestone. Stress–strain curves for 'as-collected' Solnhofen limestone, together with curves for samples heated to temperatures of 750, 810 and 1200 °C at a decarbonation progression of $\eta_{dec} = 0.12$ and $\eta_{dec} = 1.00$.

a temperature of 1200 °C we see pervasive thermal microcracking, explained by the much higher thermal expansion when compared with either 750 or 810 °C (Fig. 5).

Although it may be expected that an increased density of thermal microcracks would lead to more efficient decarbonation, due to the increased surface area for reaction, our data show that, as η_{dec} increases beyond 0.12 (i.e. into an "open" system), rock physical properties do not show a significant additional change at a constant temperature. However, we note that the increased reaction surface area may improve the efficiency of decarbonation, but, on a duration less than the minimum of 2 hr used in this study. We can infer that, at $\eta_{dec} = 1.00$, even though the rock is now fully decomposed to portlandite + lime + CO_2 gas phase (Fig. 3), the final physical properties appear largely dictated by the temperature at which the rock decarbonated (Fig. 4). These data suggest that thermal microcracking has a much greater influence on rock physical properties (porosity, ultrasonic wave velocities and elastic moduli) than the fraction of carbonate decomposed.

While some of our physical property data (porosity, ultrasonic wave velocities and elastic moduli) suggest that influence of thermal microcracking on the physical properties overwhelms the influence due to decarbonation, our UCS (unconfined compressive strength) data offer a slightly different story. Fig. 7 shows the uniaxial stress–strain curves for the samples decarbonated to $\eta_{dec} \leq 0.12$ and those decarbonated to $\eta_{dec} = 1.00$, together with the stress–strain curve for an 'as-collected' sample (UCS = 304 MPa). If we consider the data at $\eta_{dec} = 0.12$, we can see that temperature exerts a significant influence on rock strength: the UCS progressively decreases by 21, 24 and 54 per cent as the temperature is increased from 750, to 810 and to 1200 °C, respectively (Fig. 7). Since there are only small changes in sample chemistry at this stage of the reaction (Fig. 3), we can infer that the changes are likely due to thermal microcracking. However, and in spite of the fact that the analyses described in the previous paragraph indicate that the samples in Fig. 7 contain similar porosities, and have similar ultrasonic wave velocities and elastic moduli, our UCS experiments show that the progression of decarbonation after $\eta_{dec} = 0.12$ drastically reduces the compressive strength of the samples. At $\eta_{dec} = 1$, the strength reduction is significantly higher and the value of UCS decreases by 68, 71 and 91 per cent upon increasing the temperature from 750, to 810 and to 1200 °C, respectively (Fig. 7). We also note that, at both $\eta_{dec} \leq 0.12$ and $\eta_{dec} = 1$, the reduction in UCS at 750 and the 810 °C is approximately equal; however, the UCS is considerably decreased at 1200 °C. Since thermal microcracking will not increase further as decarbonation progresses at a constant temperature (the thermal microcracking should be in 'equilibrium' with the temperature, a phenomenon called the Kaiser 'temperature–memory' effect, see Heap *et al.* 2013b), the further reduction in UCS must be related to the mineralogical change from calcite to lime and portlandite. A similar inference was made by Heap *et al.* (2013a) based on the experimental data of Delle Piane *et al.* (2007). Delle Piane *et al.* (2007) showed that the decomposition product of dolomite, periclase, acted as high-shear zones in torsion experiments. The volume (calculated from unit cell values) of portlandite (i.e. 54.69 Å^3) is much lower than that of calcite (i.e. 367.85 Å^3; Xu *et al.* 2007 and references therein). In contrast to the close-packing of carbonate groups, portlandite has a hexagonal layered crystal structure of calcium oxide layers separated by hydrogen, resulting in a weak interlayer attraction. Therefore, the formation of portlandite is potentially a key factor in volcanic stability, and is strictly dependent on the presence of water. We also note that the calcite grain size increases as the temperature increases (Figs 5 and 6). In general, the compressive strength of rocks with a large grain size is lower than that for rocks with a small grain size (Guéguen & Palciauskas 1994; Paterson & Wong 2005).

4 CONCLUSIONS AND IMPLICATIONS

(i) Providing that CO_2 can be retained in the pore space of carbonate rock (i.e. a 'losed' system), the decarbonation reaction does not proceed at any magmatic pressure and temperature, excluding the direct and quick ingestion of carbonate rocks into magma (*cf.* Deegan *et al.* 2010). However, in an 'open' system, decarbonation can occur rapidly and is not hindered by carbonate rocks with a low porosity, low permeability and small grain size.

(ii) Together with CO_2 and lime, portlandite readily forms during carbonate decomposition in the presence of water (provided in this case by the ambient laboratory humidity). In nature, portlandite is commonly found in metasomatic skarns (the product of fluid–rock interaction).

(iii) Decarbonation experiments performed at different temperatures show that thermal microcracking plays a key role in the demise of rock physical properties (porosity, ultrasonic wave velocities and

elastic moduli). The magnitude of the changes in rock physical properties at low levels of decarbonation ($\eta_{dec} = 0.12$) were greatly increased as temperature was increased. At 1200 °C the rock physical properties were drastically altered. Since the chemical changes at this stage are minimal, these changes can be explained by thermal microcracking, a result of the highly anisotropic thermal expansion of calcite. It is likely that thermal microcracking is more prevalent in 'tight' rocks such as SLN. As decarbonation progressed above $\eta_{dec} = 0.12$, up to $\eta_{dec} = 1.00$, further changes in rock physical properties were very modest. From these data we surmise that thermal microcracking exerts a greater influence on rock physical properties than decarbonation.

(iv) There is a substantial reduction in UCS at low levels of decarbonation progression ($\eta_{dec} = 0.12$), also explained by the presence of thermal microcracks. However, and unlike the aforementioned physical properties (porosity, ultrasonic wave velocities and elastic moduli), decarbonation profoundly influences UCS above $\eta_{dec} = 0.12$. This can be explained by the relative weakness of lime + portlandite compared with calcite, and the increase in grain size. The presence of water and the subsequent formation of portlandite dramatically reduce the strength of metasomatic skarn rocks. Thus, metasomatic skarns created by fluid–rock interaction could therefore represent an important source of volcanic instability, especially if one considers that their petrogenetic reactions may involve a few tens of cubic kilometres (e.g. Mollo *et al.* 2011 and references therein). In contrast, magmatic skarns frequently comprise anhydrous minerals (e.g. Di Rocco *et al.* 2012 and references therein) and are therefore less prone to such chemical weakening, although their physical and mechanical properties can invariably be altered under high-temperature conditions.

(v) Our data, spanning a wide range of potential magmatic conditions, suggest that carbonate volcanic substrata are weakened on two fronts. First, and only in an 'open' system, there will be a widespread weakening due to the formation of lime and portlandite (that is not accompanied by a corresponding decrease in ultrasonic wave velocities). Secondly, in both 'open' and 'closed' systems, there will be a widespread weakening (contributing to the former) and deterioration of rock physical properties (porosity, ultrasonic wave velocities and elastic moduli) due to thermal microcracking. Additionally, and more local to the heat source (dyke or magma body), the impact of thermal cracking will be greatly increased. However, Barnes *et al.* (2005) argue that the existence of a 'closed' system is perhaps an unrealistic scenario during magma–carbonate interaction; the rocks that comprise a volcanic edifice are often highly porous and contain high microcrack densities, leaving them highly permeable (Mollo *et al.* 2012 and references therein).

ACKNOWLEDGEMENTS

S. M. was supported by the ERC Starting grant #259256 GLASS project. The authors would like to thank Thierry Reuschlé for his help in the laboratory at the Université de Strasbourg. M. J. H. and D. B. D. acknowledge the support of a Hubert Curien Partnership (PHC) PROCOPE grant (grant number 27061UE), the Deutscher Akademischer Austauschdienst (DAAD) in Germany and the Ministry of Foreign and European Affairs (MAE) and the Ministry of Higher Education and Research (MESR), both in France. D. B. D. also acknowledges a research professorship from the Bundesexzellenzinitiative (LMUexcellent) and the ERC Advanced grant 'EVOKES' (#247076). M. J. H. also acknowledges CNRS INSU grant '*Étude de la stabilité des édifices volcaniques*'.

REFERENCES

Barnes, C., Prestvik, T., Sundvoll, B. & Surratt, D., 2005. Pervasive assimilation of carbonate and silicate rocks in the Hortavær igneous complex, north-central Norway, *Lithos,* **80,** 179–199.

Beruto, D., Searcy, A.W. & Kim, M.G., 2004. Microstructure, kinetic, structure, thermodynamic analysis for calcite decomposition: free-surface and powder bed experiments, *Thermochim. Acta,* **424,** 99–109.

Bonaccorso, A., Currenti, G., Del Negro, C. & Boschi, E., 2010. Dike deflection modelling for inferring magma pressure and withdrawal, with application to Etna 2001 case, *Earth planet. Sci. Lett.,* **293,** 121–129.

Bruno, P.P.G., Cippitelli, G. & Rapolla, A., 1998. Seismic study of the Mesozoic carbonate basement around Mt. Somma–Vesuvius, Italy, *J. Volc. Geotherm. Res.,* **84,** 311–322.

Chadwick, J.P., Troll, V.R., Ginibre, C., Morga, D., Gertisser, R., Waight, T.E. & Davidson, J.P., 2007. Carbonate assimilation at Merapi volcano, Java, Indonesia: insights from crystal isotope stratigraphy, *J. Petrol.,* **48,** 1793–1812.

Chase, M.W., 1998. NIST-JANAF themochemical tables, fourth edition, *J. Phys. Chem. Ref. Data, Monograph,* **9,** 1–1951.

Chobanu, C.L. & Cook, N.J., 2004. Skarn textures and a case study: the Ocna de Fier-Dognecea orefield, Banat, Romania, *Ore Geol. Rev.,* **24,** 315–370.

Civetta, L., D'Antonio, M., De Lorenzo, S., Di Renzo, V. & Gasparini, P., 2004. Thermal and geochemical constraints on the 'deep' magmatic structure of Mt. Vesuvius, *J. Volc. Geotherm. Res.,* **133,** 1–12.

D'Antonio, M., 2011. Lithology of the basement underlying the Campi Flegrei caldera: volcanological and petrological constraints, *J. Volc. Geotherm. Res.,* **200,** 91–98.

Darroudi, T. & Searcy, A., 1981. Effect of carbon dioxide pressure on the rate of decomposition of calcite ($CaCO_3$), *J. Phys. Chem.,* **85,** 3971–3974.

Dash, S., Kamruddin, M., Ajikumar, P.K., Tyagi, A.K. & Raj, B., 2000. Nanocrystalline and metastable phase formation in vacuum thermal decomposition of calcium carbonate, *Thermochimica Acta,* **363,** 129–135.

Deegan, F.M., Troll, V.R., Freda, C., Misiti, V., Chadwick, J.P., McLeod, C.L. & Davidson, J.P., 2010. Magma-carbonate interaction processes and associated CO_2 release at Merapi Volcano, Indonesia: insights from experimental petrology, *J. Petrol.,* **51,** 1027–1051.

Delle Piane, C., Burlini, L. & Grobety, B., 2007. Reaction-induced strain localization: torsion experiments on dolomite, *Earth planet. Sci. Lett.,* **256,** 36–46.

Di Rocco, T., Freda, C., Gaeta, M., Mollo, S. & Dallai, L., 2012. Magma chambers emplaced in carbonate substrate: petrogenesis of skarn and cumulate rocks and implication on CO_2-degassing in volcanic areas, *J. Petrol.,* **53,** 2307–2332.

Dove, M.T. & Powell, B.M., 1989. Neutron diffraction study of the tricritical orientational order/disorder phase transition in calcite at 1260 K, *Phys. Chem. Min.,* **16,** 503–507.

Elliott, J.R. & Lira, C.T., 1999. *Introductory Chemical Engineering Thermodynamics,* Prentice Hall International Series, New York, 660pp.

Finger, L.W., Cox, D.E. & Jephcoat, A.P., 1994. A correction for powder diffraction peak asymmetry due to axial divergence, *J. appl. Cryst.,* **27,** 892–900.

Flowers, G.C., 1979. Correction of Holloway's (1977) adaptation of the modified Redlich–Kwong equation of state for calculation of the fugacities of molecular species in supercritical fluids of geologic interest, *Contrib. Min. Petrol.,* **69,** 315–318.

Freda, C. *et al.*, 2005. Eruptive history and petrologic evolution of the Albano multiple maar (Alban Hills, Central Italy), *Bull. Volc.,* **68,** 567–591.

Freda, C., Gaeta, M., Misiti, V., Mollo, S., Dolfi, D. & Scarlato, P., 2008. Magma-carbonate interaction: an experimental study on ultrapotassic rocks from Alban Hills (Central Italy), *Lithos,* **101,** 397–415.

Fredrich, J.T. & Wong, T.-f., 1986. Micromechanics of thermally induced cracking in three crustal rocks, *J. geophys. Res.,* **91,** 12 743–12 764.

Gaeta, M., Freda, C., Christensen, J.N., Dallai, L., Marra, F., Karner, D.B. & Scarlato, P., 2006. Time-dependent geochemistry of clinopyroxene from the Alban Hills (Central Italy): clues to the source and evolution of ultrapotassic magmas, *Lithos,* **86,** 330–346.

Gaeta, M., Di Rocco, T. & Freda, C., 2009. Carbonate assimilation in open magmatic systems: the role of melt-bearing skarns and cumulate-forming processes, *J. Petrol.,* **50,** 361–385.

Gillet, P., McMillan, P., Schott, J., Badro, J. & Grzechnik, A., 1996. Thermodynamic properties and isotopic fractionation of calcite from vibrational spectroscopy of ^{18}O-substituted calcite, *Geochim. Cosmochim. Acta,* **60,** 3471–3485.

Goff, F., Love, S.P., Warren, R.G., Counce, D., Obenholzner, J., Siebe, C. & Schmidt, S.C., 2001. Passive infrared remote sensing evidence for large, intermittent CO_2 emissions at Popocatépetl volcano, Mexico, *Chem. Geol.,* **177,** 133–156.

Guéguen, Y. & Palciauskas, V., 1994. *Introduction to the Physics of Rocks,* Princeton University Press, 294pp.

Heap, M.J., Mollo, S., Vinciguerra, S., Lavallée, Y., Hess, K.-U., Dingwell, D.B., Baud, P. & Iezzi, G., 2013a. Calcination-driven weakening of the carbonate basement under Mt. Etna volcano (Italy): implications for volcano instability, *J. Volc. Geotherm. Res.,* **250,** 42–60.

Heap, M.J., Lavallée, Y., Laumann, A., Hess, K.-U., Meredith, P.G., Dingwell, D.B., Huismann, S. & Weise, F., 2013b. The influence of thermal-stressing (up to 1000 °C) on the physical, mechanical, and chemical properties of siliceous-aggregate, high-strength concrete, *Constr. Build. Mat.,* **42,** 248–265.

Holloway, J.R., 1977. Fugacity and activity of molecular species in supercritical fluids, in *Thermodynamics in Geology,* pp. 161–181, ed. Fraser, D., Reidel.

Homand-Etienne, F. & Troalen, J.-P., 1984. Behaviour of granites and limestones subjected to slow and homogenous temperature changes, *Eng. Geol.,* **20,** 219–233.

Iacono-Marziano, G., Gaillard, F. & Pichavant, M., 2007. Limestone assimilation and the origin of CO_2 emissions at the Alban Hills (Central Italy): constraints from experimental petrology, *J. Volc. Geotherm. Res.,* **166,** 91–105.

Ingraham, T.R. & Marier, P., 1963. Kinetic studies on the thermal decomposition of calcium carbonate, *Can. J. Chem. Eng.,* **41,** 170–173.

Irving, A.J. & Wyllie, P.J., 1973. Melting relationships in CaO-CO_2 and MgO-CO_2 to 36 kilobars with comments on CO_2 in the mantle, *Earth planet. Sci. Lett.,* **20,** 220–225.

Ivanov, B.A. & Deutsch, A., 2002. The phase diagram of $CaCO_3$ in relation to shock compression and decomposition, *Phys. Earth planet. Inter.,* **129,** 131–143.

Khinast, J., Krammer, GF., Brunner, Ch. & Staudinger, G., 1996. Decomposition of limestone: the influence of CO_2 and particle size on the reaction rate, *Chem. Eng. Sci.,* **51,** 623–634.

Koster van Groos, A.F., 1982. High pressure differential analysis in the system CaO-CO_2-H_2O, *Am. Min.,* **67,** 234–237.

Langmuir, I., 1913. The Vapor Pressure of Metallic Tungsten, *Phys. Rev.,* **2,** 329–342.

Larson, A.C. & von Dreele, R.B., 1997. *GSAS: general structure analysis system,* Document LAUR 86–748. Los Alamos National Laboratory.

Le Bail, A., 2005. Whole powder pattern decomposition methods and applications: a retrospection, *Powder Diffract.,* **20,** 316–326.

Lentini, F., 1982. The geology of the Mt. Etna basement, *Memorie della Societa Geologica Italiana,* **23,** 7–25.

Lentz, D.R., 1999. Carbonatite genesis: a reexamination of the role of intrusion-related pneumatolytic skarn processes in limestone melting, *Geology,* **27,** 335–338.

Li, C.-T. & Albe, W.R., 1993. Development of an improved XRD sample holder, *Powder Diffract.,* **8,** 118–121.

Lide, D.R., Kehiaian, H.V. & Henry, V., 1994. *CRC Handbook of Thermophysical and Thermochemical Data,* CRC Press, 518pp.

Markgraf, S.A. & Reeder, R.J., 1985. High-temperature structure refinements of calcite and magnesite, *Am. Min.,* **70,** 590–600.

Masotta, M., Freda, C., Paul, T.A., Moore, G.M., Gaeta, M., Scarlato, P. & Troll, V.R., 2012. Low pressure experiments in piston cylinder apparatus: calibration of newly designed 25 mm furnace assemblies to P = 150 MPa, *Chem. Geol.,* **312–313,** 74–79.

Merle, O. & Borgia, A., 1996. Scaled experiments of volcanic spreading, *J. geophys. Res.,* **101**(B6), 13 805–13 817.

Merle, O., Barde-Cabusson, S. & van Wyk de Vries, B., 2010. Hydrothermal calderas, *Bull. Volcan.,* **72,** 131–147.

Mollo, S., Gaeta, M., Freda, C., Di Rocco, T., Misiti, V. & Scarlato, P., 2010. Carbonate assimilation in magmas: a reappraisal based on experimental petrology, *Lithos,* **114,** 503–514.

Mollo, S., Vinciguerra, S., Iezzi, G., Iarocci, A., Scarlato, P., Heap, M.J. & Dingwell, D.B., 2011. Volcanic edifice weakening via devolatilization reactions, *Geophys. J. Int.,* **186,** 1073–1077.

Mollo, S., Heap, M.J., Iezzi, G., Hess, K.-U., Scarlato, P. & Dingwell, D.B., 2012. Volcanic edifice weakening via decarbonation: a self-limiting process? *Geophys. Res. Lett.,* **39,** L15307, doi:10.1029/2012GL052613.

Ninan, K.N., Krishnan, K. & Krishnamurthy, V.N., 1991. Kinetics and mechanism of thermal decomposition of in situ generated calcium carbonate, *J. Therm. Anal.,* **37,** 1533–1543.

Norini, G., Capra, L., Groppelli, G., Agliardi, F., Pola, A. & Cortes, A., 2010. Structural architecture of the Colima Volcanic Complex, *J. geophys. Res.,* **115,** B12209, doi:10.1029/2010JB007649.

Paterson, M.S. & Wong, T.-F., 2005. *Experimental Rock Deformation: The Brittle Field,* Springer.

Peng, D.-Y. & Robinson, D.B., 1976. A new two-constant equation of state, *Ind. Eng. Chem. Fundam.,* **15,** 59–64.

Percharsky, V.K. & Zavaliji, P.Y., 2005. *Fundamentals of Powder Diffraction and Structural Characterization of Materials,* Springer Science, 713pp.

Piochi, M., Ayuso, R.A., De Vivo, B. & Somma, R., 2006. Crustal contamination and crystal entrapment during polybaric magma evolution at Mt. Somma-Vesuvius volcano, Italy: geochemical and Sr isotope evidence, *Lithos,* **86,** 303–329.

Rao, K.V., Nagender Naidu, S.V. & Satyanarayana Murthy, K., 1968. Precision lattice parameters and thermal expansion of calcite, *J. Phys. Chem. Solids,* **29,** 245–248.

Rodriguez-Navarro, C., Ruiz-Agudo, E., Luque, A., Rodriguez-Navarro, A.B. & Ortega-Huertas, M., 2009. Thermal decomposition of calcite: mechanisms of formation and textural evolution of CaO naocrystals, *Am. Min.,* **94,** 578–593.

Rosa, D.F. & Martin, R.F., 2010. A spurrite-, merwinite- and srebrodolskite-bearing skarn assemblage, West Clearwater Lake Impact Crater, Northern Québec, *Can. Min.,* **48,** 1519–1532.

Rutter, E., 1974. The influence of temperature, strain rate and interstitial water in the deformation of calcite rocks, *Tectonophysics,* **22,** 331–334.

Samtani, M., Dollimore, D. & Alexander, K.S., 2002. Comparison of dolomite decomposition kinetics with related carbonates and the effect of procedural variables on its kinetic parameters, *Thermochim. Acta,* **392–393,** 135–145.

Schubnel, A., Fortin, J., Burlini, L. & Gueguen, Y., 2005. Damage and recovery of calcite rocks deformed in the cataclastic regime, in *Geological Society Special Publications,* Vol. 245, pp. 203–221, eds Bruhn, D. & Burlini, L., Geological Society.

Siniscalchi, A. *et al.*, 2010. Insights into fluid circulation across the Pernicana Fault (Mt. Enta, Italy) and implications for flank instability, *J. Volc. Geotherm. Res.,* **193,** 137–142.

Smith, J.W., Johnson, D.R. & Muller-Vonmoos, M., 1974. Dolomite for determining atmosphere control in thermal analysis, *Thermochim. Acta,* **8,** 45–56.

Toby, B.H., 2001. EXPGUI, a graphical user interface for GSAS, *J. appl. Crystal.,* **34,** 210–213.

Treiman, A.H. & Essene, E.J., 1983. Mantle eclogite and carbonate: a possible source of sodic carbonatites and alkaline magmas, *Nature,* **302,** 700–704.

Troll, V.R., Hilton, D.R., Jolis, E.M., Chadwick, J.P., Blythe, L.S., Deegan, F.M., Schwarzkopf, L.M. & Zimmer, M., 2012. Crustal CO_2 liberation during the 2006 eruption and earthquake events at Merapi volcano, Indonesia, *Geophys. Res. Lett.,* **39,** L11302, doi:10.1029/2012GL051307.

Van Wyk De Vries, B. & Borgia, A., 1996. The role of basement in volcano deformation, *Geol. Soc. Lond. Spec. Publ.,* **110,** 95–110.

Van Wyk De Vries, B. & Francis, P.W., 1997. Catastrophic collapse at stratovolcanoes induced by gradual volcano spreading, *Nature,* **387,** 387–390.

Wang, Y. & Thomson, W.J., 1995. The effects of steam and carbon-dioxide on calcite decomposition using dynamic X-ray-diffraction, *Chem. Eng. Sci.,* **50,** 1373–1382.

Weast, R.C., 1985. *CRC Handbook of Chemistry and Physics,* 66th edn, CRC Press, 2363pp.

Wenzel, T., Baumgartner, L.P., Brügmann, G.E., Konnikov, E.G. & Kislov, E.V., 2002. Partial melting and assimilation of dolomitic xenoliths by mafic magma: the Ioko-Dovyren intrusion (North Baikal Region, Russia), *J. Petrol.,* **43,** 2049–2074.

Wohletz, K., Civetta, L. & Orsi, G., 1999. Thermal evolution of the Phlegraean magmatic system, *J. Volc. Geotherm. Res.,* **91,** 381–414.

Wu, T.C., Shen, A.H., Weathers, M.S., Bassett, W.A. & Chou, I.M., 1995. Anisotropic thermal expansion of calcite at high pressures: an in-situ X-ray diffraction study in a hydrothermal diamond-anvil cell, *Am. Min.,* **80,** 941–946.

Wyllie, P.J. & Raynor, E.J., 1965. D. T. A. and quenching methods in the system CaO-CO_2-H_2O, *Am. Min.,* **50,** 2077–2082.

Wyllie, P.J. & Tuttle, O.F., 1960. The system CaO-CO_2-H_2O and the origin of carbonatites, *J. Petrol.,* **l,** 1–46.

Xu, H., Zhao, Y., Zhang, J., Hickmott, D.D. & Daemen, L.L., 2007. In situ neutron diffraction study of deuterated portlandite $Ca(OH)_2$ at high pressure and temperature, *Phys. Chem. Min.,* **34,** 223–232.

Yavuz, H., Demirdag, S. & Caran, S., 2010. Thermal effect on the physical properties of carbonate rocks, *Int. J. Rock Mech. Min. Sci.,* **47,** 94–103.

Young, R.A., 1993. *The Rietveld Method. IUCr Monographs on Crystallography,* Oxford University Press, 298pp.

APPENDIX

When a compound S is thermally decomposed to gaseous products A and B, the equilibrium may be described by the reaction:

$$\mathrm{S(s)} \rightarrow a\mathrm{A(g)} + b\mathrm{B(g)}, \tag{A1}$$

where a and b are the number of moles of the gaseous products A and B, respectively. According to the Hertz–Langmuir equation (Langmuir 1913), a measure of the decomposition rate of compound S may be expressed through the flux of the gaseous product A, that is, J (kg m^{-2} s^{-1}), in the form:

$$J = \frac{\gamma N_{\mathrm{A}} P_{\mathrm{A}}^{\mathrm{eq}}}{(2\pi M_{\mathrm{A}} R T)^{1/2}}, \tag{A2}$$

where N_{A}, R, T and M_{A} are Avogadro's number, the gas constant (J mol^{-1} K^{-1}), the decomposition temperature (K) and the molar mass (g mol^{-1}) of the product A, respectively. Importantly, $P_{\mathrm{A}}^{\mathrm{eq}}$ is the equilibrium partial pressure (in bars) of the decomposition product A and is directly related to the thermodynamic characteristics (i.e. enthalpy and entropy) of eq. (A1). The coefficient γ is equal to 10^5 Pa bar^{-1} and represents the conversion factor from Pascals to bars.

The equilibrium constant (K_{eq}) of the decomposition reaction (A1) is related to the equilibrium partial pressure of both gaseous products A and B as follows:

$$K_{\mathrm{eq}} = P_{\mathrm{A}}^{\mathrm{eq}} \times P_{\mathrm{B}}^{\mathrm{eq}}. \tag{A3}$$

In response to the congruent decomposition of compound S during reaction (A1), the following condition obtains:

$$\frac{J_{\mathrm{A}}}{a} = \frac{J_{\mathrm{B}}}{b}. \tag{A4}$$

Substituting eq. (A2) into eq. (A4), the relationship between the equilibrium partial pressure of the products A and B may be expressed through the parameter β:

$$\beta = \frac{P_{\mathrm{B}}^{\mathrm{eq}}}{P_{\mathrm{A}}^{\mathrm{eq}}} = \frac{b}{a}\left(\frac{M_{\mathrm{B}}}{M_{\mathrm{A}}}\right)^{1/2}. \tag{A5}$$

However, the thermal decomposition of compound S may form: (i) gaseous molecules of volatile species B and (ii) low-volatility gaseous molecules of species A, which subsequently condense to form the solid product of eq. (A1) as follows:

$$\mathrm{S(s)} \rightarrow a\mathrm{A(g)} \downarrow + b\mathrm{B(g)} \uparrow \rightarrow a\mathrm{A(s)} \downarrow + b\mathrm{B(g)} \uparrow. \tag{A6}$$

If the gaseous products formed during the decomposition of S are confined within the system, eq. (A6) proceeds in 'isobaric' mode. This means that an excess of external pressure of B ($P_{\mathrm{B}}^{\mathrm{ext}}$) occurs in the system, exceeding the equilibrium partial pressure of B released during the decomposition of S. As a consequence, $P_{\mathrm{B}}^{\mathrm{ext}} \gg P_{\mathrm{B}}^{\mathrm{eq}}$ and $P_{\mathrm{B}}^{\mathrm{ext}}$ remains constant over the decomposition reaction (A6). Under isobaric conditions, the equilibrium partial pressure of A is:

$$P_{\mathrm{A}}^{\mathrm{eq}} = \frac{K_{\mathrm{eq}}^{1/a}}{\left(P_{\mathrm{B}}^{\mathrm{ext}}\right)^{b/a}}. \tag{A7}$$

If we consider eqs (A2), (A5) and (A7), we can see that J is inversely proportional to $(P_{\mathrm{B}}^{\mathrm{ext}})^{b/a}$ and, if $a = b = 1$, the following relationship is obtained:

$$J \propto \frac{1}{P_{\mathrm{B}}^{\mathrm{ext}}}. \tag{A8}$$

Eq. (A8) indicates that, at the equilibrium interface between the coexisting solid S and the gaseous phase B, the thermal decomposition rate of reaction (A6) decreases when the partial pressure of the product B increases in the external atmosphere.

For calcite, the thermal decomposition of $CaCO_3$ produces gaseous molecules of CO_2 and low-volatility gaseous molecules of CaO, which subsequently condense to form solid CaO:

$$\mathrm{CaCO_3(s)} \rightarrow \mathrm{CaO(s)} \downarrow + \mathrm{CO_2(g)} \uparrow \tag{A9}$$

The decarbonation reaction (A9) proceeds in response to the formation of: (i) a first interface between $CaCO_3$ and CaO, where calcium cations + oxygen groups are still arranged in the original positions they occupied in the hexagonal calcium carbonate lattice and (ii) a second interface between calcium cations + oxygen groups and condensed cubic CaO, which has recrystallized to its stable crystal habit (Ingraham & Marier 1963), that is, the condensation of gaseous product A described by eq. (A6). In fact, there is crystallographic control in the advancement of the $CaCO_3$ (reactant)–CaO (product) interface (Rodriguez-Navarro *et al.* 2009). The thermal decomposition starts at the external surface of a calcite crystal by forming a reactant–product interface through which the CO_2 can diffuse; as the reaction progresses the interface moves towards the core of the grain (Beruto *et al.* 2004). Since the CO_2 is released through the first interface between $CaCO_3$ and CaO, a pressure gradient ($\Delta P_{\mathrm{CO_2}}$) develops across it that can be expressed as follows:

$$\Delta P_{\mathrm{CO_2}} = P_{\mathrm{CO_2}}^{\mathrm{eq}} - P_{\mathrm{CO_2}}^{\mathrm{ext}}, \tag{A10}$$

where $P_{\mathrm{CO_2}}^{\mathrm{eq}}$ is the equilibrium pressure between the crystal surface and the external atmosphere.

Eq. (A10) describes the decomposition of a single calcite crystal; the decarbonation reaction rate of a rock cannot be estimated through $P_{\mathrm{CO_2}}^{\mathrm{eq}}$ due to the presence of multiple crystals and, therefore, a large number of reaction interfaces. In particular, at the

grain-scale of a rock, $P^{eq}_{CO_2}$ will depend on: (i) the heat and mass transfer rates across each reaction interface, (ii) the particle/grain size, (iii) the pore geometry and (iv) the thermodynamic stability of each reaction product. As described by eq. (A8), the conversion of $CaCO_3$ to CaO is strictly dependent on the $P^{ext}_{CO_2}$ of the system which, in turn, is the main rate-limiting factor of decarbonation reaction (A9), irrespective of the volume of carbonate material and the particle size of its grains (Smith *et al.* 1974; Darroudi & Searcy 1981; Wang & Thomson 1995; Khinast *et al.* 1996). Moreover, from a thermodynamic point of view, it is the fCO_2 rather than $P^{ext}_{CO_2}$ that is the 'chemical' pressure governing the chemical equilibrium of reaction (A9).

When magmas interact with carbonate rocks in volcanic and plutonic systems, the fCO_2 strictly controls the amount of $CaCO_3$ decomposed (Barnes *et al.* 2005), the total final pressure (Wenzel *et al.* 2002) and the oxygen fugacity (fO_2) of the system (Gaeta *et al.* 2009; Di Rocco *et al.* 2012). This means that, similar to the case of decomposition rate of a single calcite crystal, the decomposed fraction of a carbonate rock (η_{dec}) is inversely proportional to the fCO_2:

$$\eta_{dec} \propto \frac{1}{fCO_2}. \tag{A11}$$

According to eq. (A2), η_{dec} is also inversely proportional to both the reaction temperature and the time (t):

$$\eta_{dec} \propto \frac{1}{T}, \tag{A12}$$

$$\eta_{dec} \propto \frac{1}{t}. \tag{A13}$$

The value of η_{dec} ranges from 0 to 1 and is calculated as follows:

$$\eta_{dec} = \frac{m_x}{m_f}, \tag{A14}$$

where m_f is the total mass of CO_2 of a carbonate rock prior to thermal decomposition and m_x is the mass of CO_2 released during $CaCO_3$ decomposition at a specific fCO_2, T and t. Thus, according to the stoichiometry of reaction (A9), η_{dec} can be readily used to describe the progression of carbonate decomposition in a rock. For example, at ambient pressure in an 'open' system (gaseous products are free to escape), pure carbonate rocks generally starts to decompose at $\sim$700 °C (e.g. Mollo *et al.* 2011 and references therein). At this latter temperature, the carbonate rock is fully decomposed, the CO_2 measured via the reaction is $\sim$44 wt. per cent, and $\eta_{dec} = 1$.

SUPPORTING INFORMATION

Additional Supporting Information may be found in the online version of this article:

Table S1. Experimental conditions used for low pressure (Experimental Set 1) and high pressure (Experimental Set 2) experiments (http://gji.oxfordjournals.org/lookup/suppl/doi:10.1093/gji/ggt265/-/DC1).

Please note: Oxford University Press is not responsible for the content or functionality of any supporting materials supplied by the authors. Any queries (other than missing material) should be directed to the corresponding author for the article.